Green Chemistry

Renewable Linear Alpha-Olefins by Base-Catalyzed Dehydration of Biologically-Derived Fatty Alcohols

Journal:	*Green Chemistry*
Manuscript ID	GC-ART-01-2021-000243.R1
Article Type:	Paper
Date Submitted by the Author:	23-Apr-2021
Complete List of Authors:	McClelland, Daniel; University of Wisconsin - Madison, Chemical and Biological Engineering Wang, Bo-Xun; University of Wisconsin, Chemical and Biological Engineering Cordell, William; University of Wisconsin, Chemical and Biological Engineering Cortes-Pena, Yoel; University of Illinois at Urbana-Champaign Gilcher, Elise; University of Wisconsin, Chemical and Biological Engineering Zhang, Lifeng; University of Wisconsin, Chemical and Biological Engineering Guest, Jeremy; University of Illinois at Urbana-Champaign, Civil & Environmental Engineering Pfleger, Brian; University of Wisconsin, Chemical and Biological Engineering Huber, George; University of Wisconsin, Chemical and Biological Engineering Dumesic, James; University of Wisconsin Madison, Chemical and Biological Engineering

Renewable Linear Alpha-Olefins by Base-Catalyzed Dehydration of Biologically-Derived Fatty Alcohols

Daniel J. McClelland[a,b], Bo-Xun Wang[a,b], William Cordell[a,b], Yoel Cortes-Peña[c], Elise B. Gilcher[a], Lifeng Zhang[a], Jeremy S. Guest[c], Brian F. Pfleger[a,b], George Huber [a,b,*], and James A. Dumesic[a,b]

[a] Department of Chemical and Biological Engineering, University of Wisconsin-Madison, Madison, WI, USA.
[b] DOE Center for Advanced Bioenergy and Bioproducts Innovation, University of Wisconsin-Madison, Wisconsin, USA
[c] Department of Civil and Environmental Engineering and DOE Center for Advanced Bioenergy and Bioproducts Innovation (CABBI), University of Illinois at Urbana-Champaign, Urbana, Illinois, USA
*corresponding author, email: gwhuber@wisc.edu

Abstract

Base catalysts were studied for the dehydration of fatty alcohols to linear alpha olefins (LAOs). For the gas phase dehydration of 1-octanol to 1-octene, 15%Cs/SiO_2 catalyst was 56% selective at 10% conversion. Diluting a feed of C_8, C_{10}, and C_{14} fatty alcohols to 50% in undecane increased the selectivity to alpha olefins to 77-99%. 15%Cs/SiO_2 was further investigated for the gas phase dehydration of a 4.2 g/L mixed C_8-C_{14} fatty alcohol in tridecane feed and showed linear alpha olefin selectivities of 78-100% at initial conversions of 51-91% with the conversion lowering to 32-77% over 30 h. Catalytic activity was totally regenerated through calcination. A feed of biologically derived alcohols was produced with *E. coli* strain CM24 transformed with three plasmids (pBTRCk – pVHb – maACR, pACYC – pVHb – seFadBA, pTRC99A – pVHb – tdTER – fdh) which yielded a 5.5 g/L of C_8-C_{14} fatty alcohol in tridecane. This biologically-derived feed was successfully dehydrated to linear alpha olefins over 15%Cs/SiO_2 at selectivities of 60-100% with initial conversions of 35-75% which decreased to 22-55% over 30 h. Techno-economic analysis (TEA) of the integrated process for fatty alcohol production and subsequent dehydration to alpha olefins was conducted across the potential fermentation TRY (titer, rate, yield) landscape. Baseline fermentation performance resulted in a minimum product selling price (MPSP) double the market price for LAOs due to low titers and high costs associated with managing water and tridecane solvent flows through the system. However, targ10-eted improvements in fermentation performance (e.g., achieving 40 g/L titer, 0.5 g/L/h productivity, 80% theoretical yield) can enable financially viable production of biologically derived LAOs.

Introduction

Linear alpha olefins (LAOs) are widely used for the production of plasticizers, surfactants, lubricants, and polyethylene comonomers.[1-3] The major global use of LAO is for the production of polyethylene co-monomers, including linear low density polyethylene (LLDPE), high density polyethylene, and elastomers. This increasing demand for polyethylene comonomers has contributed to projections of annual LAO market growth of >4% from 2019-2024.[4] The commercial production of LAOs has been developed over decades from petroleum feedstocks[5, 6] through two main catalytic routes, oligomerization of ethylene and separation of Fischer–Tropsch Synthesis products.[7, 8] The former process is based on Ziegler chemistry, which uses triethyl-

aluminum to catalyze the chain growth of alpha olefins. The latter process involves the reaction of syngas to form large alkanes and olefins. These processes generally produce a distribution of LAOs with chain lengths from 4 to 22 that follow a Schulz-Flory distribution where the final distribution is dependent on the chain growth. However, there is more market demand for LAOs ranging from C_6 to C_{10} due to the growth in demand of LLDPE.[4] Prior to the introduction of the Ziegler chemistry, LAOs were produced commercially by dehydration of biomass-derived alcohols over base catalysts where the alcohols were produced from fatty acid triglycerides (through trans-esterification followed by hydrogenation).[9] This approach primarily produced C_{16} and C_{18} olefins with very high purity. The last of these commercial facilities, which was operated by Archer-Daniels-Midland, was shut down in 1966 due to high production costs compared to the Ziegler approach. With recent efforts to move society toward a circular economy, there is renewed interest in the production of LAOs from renewable resources.[10]

C_4-C_{16} fatty alcohols can be produced by microbial catalysts fed carbohydrates.[11-13] In nature, some microbes produce modest amounts of fatty alcohols for incorporation into wax esters that provide biological functions including energy/storage compounds, anti-desiccation properties, and toxin resistance.[14] Fatty alcohols are synthesized by enzymatically reducing the carbonyl of acyl-thioester or fatty acid metabolites present in lipid metabolism. Microbes can synthesize fatty alcohols via fermentation (i.e., anaerobic cultivation that couples fatty alcohol production to substrate uptake) or aerobic cultivation to leverage the strong driving force of fatty acid biosynthesis (which requires respiration to compensate for elevated ATP demand). Elevated production of specific fatty alcohols (e.g., with desired chain lengths) has been accomplished by applying metabolic engineering to the native lipid metabolism of industrially relevant microbes such as *Escherichia coli*,[15-18] *Yarrowia lipolytica*,[13] and *Saccharomyces cerevisiae*.[19] These efforts generally consist of 1.) genetic modifications to elevate flux through fatty acid biosynthesis or thiolase mediated β-reduction, 2.) heterologous expression of acyl-thioester reductases and/or aldehyde reductases to enable production of fatty alcohols, 3.) genetic disruption of pathways that compete with production of fatty alcohols, and 4.) expression of enzymes to target flux to desired fatty alcohol species. Each of these fatty alcohol production strategies could serve as a biological source of fatty alcohols for further catalysis.

The fatty alcohols can be converted into LAOs via metal-catalyzed dehydration reactions.[20] Several solid acid zeolite catalysts have been proposed for facilitating alcohol dehydration reactions, such as HSZM-5[21, 22] and SAPO-34.[23, 24] Moreover, metal-containing mesoporous acid catalysts have been studied for dehydrating alcohols into corresponding olefins, such as Ni-MCM-41[25, 26] and Zr-KIT-6.[27, 28] They are all highly active for catalyzing alcohol dehydration reactions, however, acid catalysts cannot selectively produce LAOs since the acid sites will catalyze double-bond isomerization.[29, 30] Therefore, to produce LAOs selectively, acid sites need to be reduced or removed to minimize the extent of isomerization. Yamamoto *et al.* neutralized acid sites on the surface of zirconium oxide though loading sodium hydroxide on zirconium oxide,[31] finding that this method can promote the formation of alpha olefins in alcohol dehydration reactions.

Base catalysts have been reported to catalyze primary alcohol dehydration to LAOs since they can favor the formation of the double bond in the alpha position while limiting isomerization.[32, 33] Solinas *et al.* used the solid base catalyst CeO_2-ZrO_2 for the conversion of 4-methylpentan-2-ol, a secondary alcohol, into 4-methylpent-1-ene.[34] The 1-alkene selectivity values were observed to range between 84 and 59% for different Ceria catalyst loadings (0, 25, 50, 75, and 100 mol%). Thomasson *et al.* prepared the solid base catalyst, cesium-modified MgO catalyst, which gave rise to high selectivity (>80%) for the conversion of 2-butanol to 1-butene.[35]

Tsukamoto *et al.* made the solid base catalyst, SiO_2-supported cesium dihydrogen phosphate, showing over 90% of selectivity of 2,3-butanediol to 1,3-butanediene.[36] However, base catalysts have not been studied for converting medium chain fatty alcohols into LAOs. One exception to this is when we previously studied the selective gas phase dehydration of 1-octanol to 1-octene with a supported 15%Cs/SiO_2 catalyst with a selectivity of 99% at 5% conversion.[33] CeO_2, and Yb_2O_3 have been shown to be selective for production of LAOs from secondary alcohols.[37]

In the present work, we investigate base catalysts, 15%Cs/SiO_2, CeO_2, and Yb_2O_3, for the gas phase dehydration of biologically derived medium chain primary alcohols (C_8-C_{14}). For this work, a 15% Cs loading was selected to follow the work of Brentzel et al. while CeO_2, and Yb_2O_3 were used as purchased. Additionally, SiO_2 was used as an inert support to understand the catalytic role of the Cs. Other supports may be beneficial to the activity or selectivity of the reaction. The reaction was carried out in the gas phase to prevent any mass transfer problems that could occur in the liquid phase to effectively increase the turnover frequency for catalyst. Investigations with these catalysts will start with a neat 1-octanol feedstock, showing the feasibility of the process without solvents before demonstrating the process with a blend of higher chain length alcohols in alkane solvents. Finally, the dehydration of biologically-derived fatty alcohols (C_8 to C_{14}) was performed to identify the impurities that can poison the catalysts. Catalysts were characterized before and after reactions with CO_2 TPD and NH_3 TPD for acid/base sites counts for all catalysts and STEM and XPS were carried out for the supported catalyst, 15%Cs/SiO_2, to obtain the particle size distribution and the cesium oxidation state on the catalyst surface. Finally, the experimental results are leveraged to characterize the economic feasibility of our approach and set performance targets via integrated biorefinery design, process modeling, and techno-economic analysis (TEA). Combining experimental research with TEA is common and beneficial for evaluating the economic viability of new processes by determining experimental milestones required for future process scaling.[38-45]

This paper is the first report on the integration of the biological production of fatty alcohols with the catalytic dehydration of fatty alcohols into linear alpha olefins (LAOs) and then combining this into a process study to estimate the economic feasibility of this approach. This paper provides a detailed understanding of the economics and areas for improvement for the production of green LAOs. This is an area that is receiving tremendous interest from both academia and industry as the chemical industry attempts to move to a circular economy.

Experimental

Catalyst Preparation

The approximately 15 wt% cesium catalyst was supported on an acid washed silica through incipient wetness impregnation. The silica was acid washed prior to use to remove trace minerals. For acid washing, 15 g of silica was added to a round bottom flask with a solution of 700 mL of deionized water and 4.8 mL of 70% HNO_3 which was stirred for 3 h at 700 rpm. After stirring, the solution was vacuum filtered with an additional 2 L of deionized water to remove any remaining HNO_3 and dried in an oven at 110ºC overnight. For the incipient wetness impregnation, the acid washed silica was found to have approximately 1.1 mL/g pore volume. The precursor solution was prepared by dissolving approximately 2.55 g of cesium acetate in 11 g deionized water. The precursor solution was then added dropwise to 10 g of the acid washed silica while stirring to break up any clumps until the entirety of the precursor solution was added which left the silica at the incipient point. The resulting catalyst was left in a 110ºC oven overnight (~16 h) to dry. It was found that the duration of this drying could have an effect on the resulting catalyst. After drying,

the catalyst was calcined under air flow. Under 100 mL/min air, the catalyst was heated over 1 h to 120ºC and held for 4 h to insure it was completely dry. Following that, it was further heated to 450ºC over 2 h and held for 16 h after which it was allowed to cool back to room temperature. The CeO_2 (add vendor) and Yb_2O_3 (add vendor) were purchased and similarly calcined prior to use.

Gas phase dehydration

The gas phase dehydration experiments were performed in a downflow continuous flow reactor. Prior to reaction, the catalyst was packed into a reactor tube and held in place in the reactor tube by quartz wool. Silica chips were used to fill any extra void space above and below the catalyst bed and were also held in place by quartz wool. The catalyst was pretreated with the following conditions: under 50 mL/min He the catalyst is heated to 400ºC over 3 h and held for 1 h before being lowered to the reaction temperature of 350ºC. For the experiments, the liquid feeds were pumped in with an HPLC pump where they were vaporized in a preheating zone with a sweep gas prior to entering the heating zone. After passing through the catalyst bed in the heating zone, they were passed through a condenser and collected in a chilled collection vessel. The purge gas then passes through a backpressure regulator which keeps the reactor above atmospheric pressure. Typical conditions for reactions with neat 1-octanol were 0.02 mL/min feed flowrate, 350ºC heating zone, 25-50 mL/min He purge gas, 1 g catalyst, 200ºC preheating zone, 0ºC condenser, and 65 psia backpressure. The preheating zone and condenser temperatures were increased to 300ºC and 6ºC respectively when using the mixed alcohol feed (1-octanol, 1-decanol, 1-dodecanol, and 1-tetradecanol in a tridecane solvent). This was due to the higher melting and boiling points of the higher alcohols and tridecane solvent. The catalyst amounts were decreased to 50 mg due to the significantly lower concentrations of the 1-alkanols in the tridecane solvent. Samples were collected every hour for 6 hours where steady state was typically reached after 3 hours. Products were quantified with a Shimadzu GC-2010 equipped with a ZB-5HT column and flame ionization detector under the following ramp: 40ºC hold for 5 min, 7.5ºC ramp to 300ºC with a 4 min hold. Concentrated samples were diluted in acetone to approximately 2.5 wt% prior to analysis. Dilute samples in tridecane were analyzed as is while standards were made in both acetone and tridecane and used for the corresponding samples.

The mass balance, carbon balance, conversion, and selectivity of each sample were calculated from the mass and molar flowrates of each species determine by laboratory analytical balances and GC-FID analyses. Mass balances for each sample were calculated with through Equation 1:

$$mass\ balance = m_{sample}/(\dot{m}_{average} * t_{sample}) \quad \text{(Equation 1)}$$

Where m_{sample} is the mass of the sample, $\dot{m}_{average}$ is the average mass flowrate fed during the experiment, and t_{sample} is duration of the sample. The carbon balance of the reactants each sample were calculated with the Equation 2:

$$carbon\ balance = \sum(\dot{n}_{i,p} * C_i)\ /\sum(\dot{n}_{i,f} * C_i) \quad \text{(Equation 2)}$$

Where $\dot{n}_{i,p}$ is the molar flowrate of each species *i* in the product stream, C_i is the carbon content of each species *i*, $\dot{n}_{i,f}$ is the molar flowrate of each species *i* in the feed, and MW_i is the molecular weight of each species *i.* The conversion and selectivity were calculated for each sample by Equations 3 and 4:

$$conversion = \dot{n}_{r,p}/\dot{n}_{r,f} \quad \text{(Equation 3)}$$

$$selectivity_i = \frac{\dot{n}_{i,p}}{\dot{n}_{r,f} - \dot{n}_{r,p}} \quad \text{(Equation 4)}$$

Where $\dot{n}_{r,p}$ and $\dot{n}_{r,f}$ are the molar flowrates of the reactant in the product stream and feed and $\dot{n}_{i,\,p}$ is the molar flowrate of species *i* in the product stream.

Catalyst Characterization

Temperature Programmed Desorption (TPD)

A TPD setup was utilized for performing CO_2 and NH_3 TPD. For CO_2 TPD, the catalyst was pretreated in 50 mL/min of He with a 1ºC/min ramp to 400ºC with a 60 min hold. Dosing was carried out after catalyst was cooled to 40ºC, where 10% CO_2 in He was dosed at 50 mL/min for 1 h. After dosing, the catalyst was purged with 50 mL/min He for 1 h at 40ºC before the temperature ramp was carried out. The catalyst was ramped to 700ºC with 50 mL/min He at 10ºC/min with a 1 h hold at 700ºC. NH_3 TPD was carried out in a similar manner with minor changes. The catalyst was pretreated in an identical manner. Dosing was performed at 150ºC with 50 mL/min 10% NH_3 in He for 1 h with a purged of 50 mL/min He for 1 h at 150ºC before the temperature ramp. Similarly, the catalyst was ramped to 700ºC with 50 mL/min He at 10ºC/min with a 1 h hold at 700ºC. Throughout the pretreatment, dosing, purging, and ramp, the vapor phase effluent was continuously sampled with the mass fragments of 4, 15, 16, 17, 18, and 44 for on a mass spectrometer (Pfeiffer Vacuum, Omnistar) for He, H_2O, CO_2, and NH_3 quantification. H_2O was tracked to insure it did not erroneously contribute to NH_3 quantification.

Scanning transmission electron microscopy (STEM)

STEM imaging was employed to perform a particle size distribution analysis on a FEI Titan Stem with Cs aberration correction operated at 200 kV in high-angle annular dark field (HAADF) mode. The 15% Cs/SiO2 catalyst was passivated and deposited onto a holey carbon coated copper grid by dispersion in ethanol and subsequent grinding in a mortar to suspend the catalyst powder. The sample was plasma cleaned before loading into the microscope.

X-ray Photoelectron Spectroscopy (XPS)

A K-alpha XPS (Thermo Scientific) instrument with a micro-focused monochromatic Al Kα X-ray source was used to measure the surface composition and chemical state of the catalysts. Typically, 100 mg of sample was loaded into a Schlenk tube and under 50 mL/min He over 3 h was heated to 400ºC with a 1 h hold. The tube was transferred to glovebox and the sample was mounted on a transfer vessel (Transfer Vessel K-Alpha), which was then transferred to the XPS chamber. The entire procedure was operated without exposing the catalyst to air or moisture. The spectra in the Cs 3d, C 1s, and Si 2p regions were collected with 10 scans, 100 ms dwell time, and 0.02 eV energy step size. The binding energy scale was calibrated using the Si 2p feature at 103.3 eV.

Alcohol Production Culture

Microbial production of fatty alcohols was performed as described in Mehrer et. al. with minor adjustments.[18] *E. coli* strain CM24 was transformed with three plasmids (pBTRCk – pVHb – maACR, pACYC – pVHb – seFadBA, pTRC99A – pVHb – tdTER – fdh) that enable fatty alcohol production. Cells were cultured for 96 hours in triplicate 125mL serum vials containing 75mL of media (Lysogeny broth supplemented with 1% glucose, 34 µg/mL chloramphenicol, 100µg/L carbenicillin, and 50 µg/mLkanamycin and a 20% v/v tridecane overlay). Tridecane was added to provide a product sink for the fatty alcohols and facilitate downstream separation. Cultures were inoculated with to a starting optical density of 0.05 using cultures grown overnight

from single colonies. At harvest, cultures were cooled on ice for 1 hour before isolation of the tridecane overlay by centrifugation (3000 x g for 15 min). Emulsions of tridecane and media were broken by cycles of freeze-thawing at -80°C followed by additional centrifugation. Tridecane samples were analyzed by GC-FID to quantify alcohol concentration as described previously. Post-analysis, samples were combined to provide sufficient volume for catalytic dehydration studies.

Technoeconomic Analysis

The financial viability of the proposed process was evaluated for the production of 150,000 tons·yr^{-1} of LAOs using BioSTEAM.[46] The plant size is well within the expected North American market growth for LAOs of >970,000 ton·yr^{-1} between 2019-2024.[4] The process is divided into five sections: fermentation, 3-phase decanter centrifuge, dehydration, separation, and outside boundary limits (OSBL) (Figure 1). The stream tables with process flow diagrams in each area are available in Tables S42-S51 and Figures S3-S7 in the ESI. LAOs are fractionated by chain length to be sold as pure chemicals at 97% purity, consistent with industrial production processes which typically produce LAOs between 94-99% purity (e.g., Exxon's ethylene oligomerization process, DuPont's Versipol process).[4]

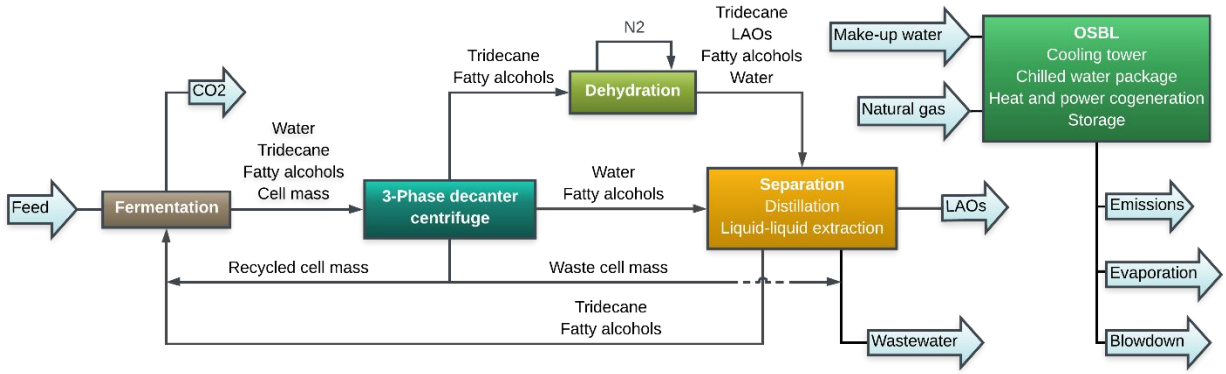

Figure 1. Simplified flowsheet depicting the five main areas of the LAO production process. A mixture of glucose, growth nutrients, water, and tridecane is mixed and fed to fermentation. The fermenter effluent is sent to a 3-phase decanter centrifuge to separate the oil, aqueous, and cell mass fractions. The cell mass is partially recycled to the fermenter, the oil fraction is sent to dehydration, and the aqueous fraction is sent to the separation section to recover fatty alcohols by liquid-liquid extraction. The effluent of the dehydration section is also sent to the separation section to recover the LAOs by distillation. OSBL unit operations include storage, a cooling tower, a chilled water package, and heat and power cogeneration.

The fermenter is modeled by specifying the fraction of theoretical yield (Equation S1 in the ESI), with any remaining glucose consumed for cell growth (Equation S2 in the ESI). Tridecane is used as an oxygen vector and a solvent for the fermentation products in the fermentation broth. The fermentation is selective for hexanol, octanol, and decanol to simplify the downstream separation scheme to distill the lighter LAOs from the heavy tridecane solvent. If longer chain lengths are produced, a large amount of tridecane would need to be distilled from the heavier LAOs, a capital and utility intensive process. Thus, an alternative process configuration implementing liquid-liquid extraction may be more suitable if longer chain lengths are produced. Corn steep liquor (CSL) and diammonium phosphate (DAP) are fed as affordable sources of nitrogen and phosphate for cell growth.[47] Details on product formation, cell growth, and the concentration of all chemicals in the fermenter broth are described in the ESI (Table S1).

Detailed TEA results were evaluated for two scenarios: 1.) a baseline fermentation performance scenario with conservative assumptions about full-scale performance (3.5 $g \cdot L^{-1}$ titer, 50% theoretical yield, 0.1 $g \cdot L^{-1}hr^{-1}$ productivity), and 2.) a target scenario which assumes the fermentation technology operates at industrially feasible performance targets (40 $g \cdot L^{-1}$ titer, 80% theoretical yield, 0.5 $g \cdot L^{-1}hr^{-1}$ productivity). The price of glucose (the main feedstock) was assumed to be the average production cost of cellulosic sugar from corn stover using the dilute acid pretreatment method (190 $USD \cdot ton^{-1}$), with an added cost of 54 $USD \cdot ton^{-1}$ for the addition of both an evaporator and a condenser to concentrate sugars to 487 $g \cdot L^{-1}$.[47, 48] To account for the sensitivity of the minimum product selling price (MPSP) to the unit cost of glucose, the unit cost was treated as uncertain with a triangular probability density function (minimum, most probable, and maximum values of 150, 240 and 350 $USD \cdot ton^{-1}$). The algorithms used for designing, modeling, and estimating unit operation costs can be found in Tables S2 and S3 (ESI). Additional details on the design, utility requirements, purchase costs, and installed equipment costs of all unit operations can be found in Tables S8-S41 (ESI). All TEA parameters follow assumptions made for the production of cellulosic ethanol from corn stover.[47] The price of the dehydration catalyst, 9.69 $USD \cdot kg^{-1}$, was estimated through CatCost™, a catalyst estimation tool.[49] A complete breakdown of the estimated capital and operating expenditures, including variable and fixed operating costs, can be found in Tables S4-S7 (ESI). A breakdown of the discounted cash flow analysis can be found in Tables S52 and S53 (ESI).

Results and Discussion

Fermentation of Carbohydrates to Medium-chain Fatty Alcohols

In prior work, *E. coli* was engineered to produce medium-chain fatty alcohols via a thiolase-mediated fermentation.[18] The primary strain CM24, was cultured under conditions to better integrate fatty alcohol production with subsequent extraction and dehydration catalysis. Dodecane and similar alkanes have been used to facilitate separation of aliphatic products from microbes and decrease product toxicity. Given the similar retention times of dodecane and 1-dodecanol dehydration products, we elected to use tridecane as the extraction-phase in the culture. For each catalytic run, six cultures of CM24 were grown in 125 mL serum vials with 75 mL of LB supplemented with 10 g/L glucose, appropriate antibiotics, and a 20% (v/v) tridecane overlay. After four days of fermentation, the tridecane overlay was separated from the aqueous cultures and combined to provide material for dehydration studies. The typical titer of fatty alcohols produced in each sample was 5.5 g/L and 35% of the apparent theoretical yield on the glucose fed to cells. The concentrations of the C8-C14 fatty alcohols, acetic acid esters, and fatty acids are shown in Table 1.

Table 1. Concentrations of products in the biologically derived feed, including fatty alcohols, acetic acid esters, and fatty acids.

Biologically Derived Feed	
Compound	Concentration (g/L)
1-octanol	0.57
1-decanol	1.74
1-dodecanol	2.02
1-tetradecanol	1.18
Acetic acid esters	0.29
Fatty Acids	0.18

Gas phase dehydration of neat 1-octanol

1-octanol dehydration was studied with 15%Cs/SiO_2, CeO_2, and Yb_2O_3 catalysts as shown in Table 2. The 15%Cs/SiO_2 was the most selective to 1-octene at 38% at a 1-octanol conversion of 17%. The CeO_2 and Yb_2O_3 catalysts had low 1-octene selectivities (less than 4%). The 15%Cs/SiO_2 catalyst had one detectable side-product, octanal, at 4% selectivity while CeO_2 produced octanal at 2% as well as 8-pentadecanone at 17% and octyl octanoate at 16% selectivity. Yb_2O_3 had only one detectable side-products, octyl octanoate, at 2% selectivity. It was evident that all three catalysts were facilitating side-reactions since their carbon balances were 89-90% based on the products with 96-99% mass balances to liquid products leading to selectivity of known products of 41% or lower.

Figure 2 shows the proposed reaction pathway for the 1-octanol conversion over base catalysts. The 1-octanol is dehydrated to 1-octene and water over all three catalysts while isomerization of 1-octene to 2-, 3-, and 4-octene was limited. The side products are likely produced through the condensation of octanal which is in equilibrium with 1-octanol. Over base catalysts, octanal can react with itself through esterification or aldol condensation. The esterification product, octyl octanoate is directly observed over CeO_2 and Yb_2O_3 while aldol condensation is observed through 8-pentadecanone over CeO_2 which would form through an aldol condensation + hydride shift + retro-aldol condensation route as has been demonstrated of through the formation of acetone from ethanol over CeO_2.[50, 51] Aldol condensation occurs over base catalysts and the C_{16} aldol condensation product is likely to be the cause for the missing selectivity for all three catalysts. Octanal formation and octanal condensation reactions need to be inhibited to increase the 1-octene selectivity.

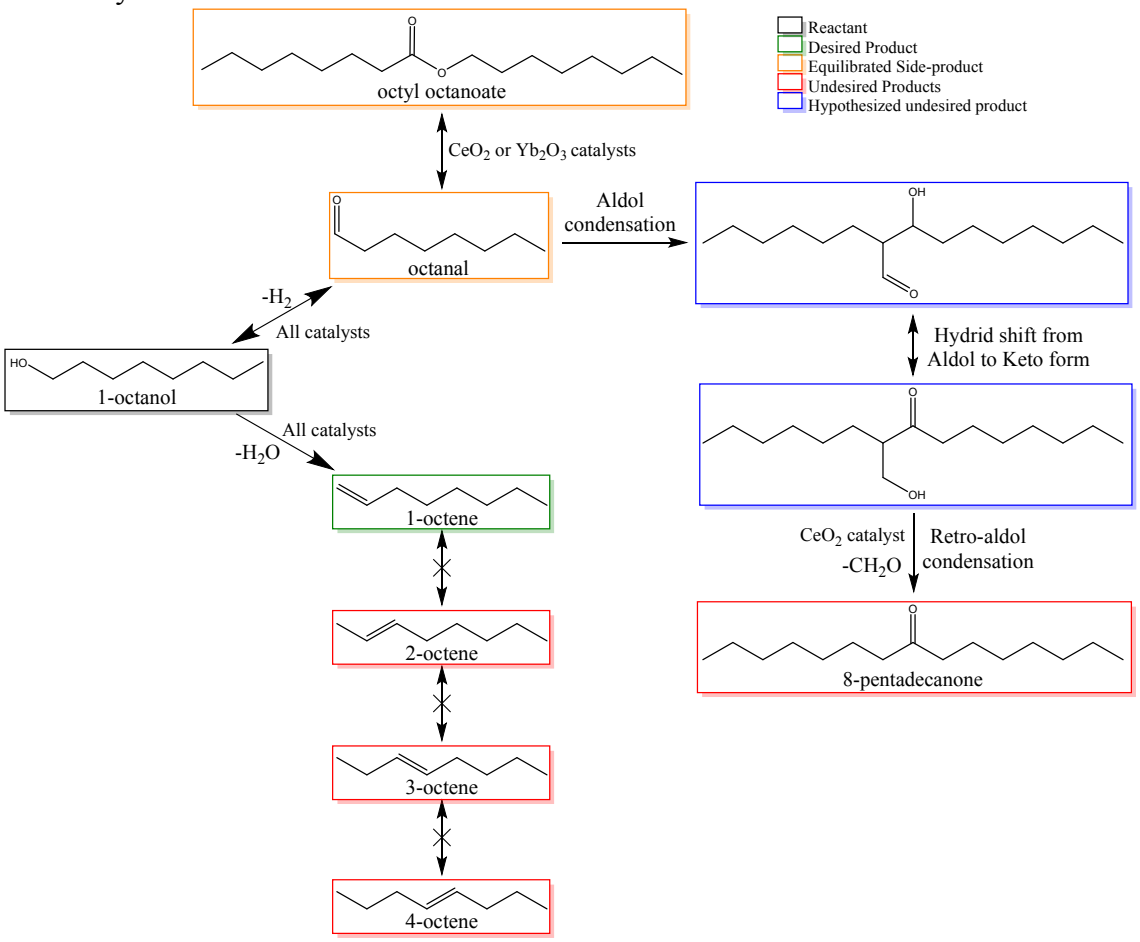

Figure 2. Reaction pathways of alcohol reactions over base catalysts. All labeled compounds were identified by GC-MS and confirmed with standards in GC-FID.

We hypothesized that by adjusting the 1-octanol/octanal equilibrium we could decrease the octanal selectivity and condensation products. This was done by introducing a H_2 cofed during the reaction. Over 15%Cs/SiO_2, the conversion decreased from 17% to 15% while the selectivity to 1-octene increased from 38% to 51% and the octanal selectivity increased from 4% to 20%. This was surprising since the H_2 was cofed to decrease octanal selectivity. This indicates that hydrogen inhibits the octanal condensation reactions to a larger degree than the octanal formation. This

increased the selectivity to known products from 41% to 74% for the 15%Cs/SiO_2 catalyst. Hydrogen did not change the activity or selectivity of the CeO_2 catalyst. However, the octanal selectivity increased from 2% to 14%. The 8-pentadecanone and octyl octanoate selectivity also increased from 17% to 25% and 16% to 44% respectively and octane was formed with a 1% selectivity. Hydrogen addition increased the selectivity to known products from 39% to 88% and increased the carbon balance from 89% to 98% over 89%. Yb_2O_3 also had selectivity change with hydrogen and a decrease in conversion from 11% to 10%. The 1-octene selectivity varied slightly, decreasing from 3% to 2% while octyl octanoate selectivity increased from 2% to 9%.

15%Cs/SiO_2 had the highest 1-octene selectivity of the catalyst tested. As long as 1-octanal does not undergo condensation reactions it will be converted into 1-octene. We can therefore calculate a normalized 1-octene selectivity of 64% according to Equation 5.

$$normalized\ selectivity_i = \frac{\dot{n}_{i,p}}{\dot{n}_{r,f} - (\dot{n}_{r,p} + \dot{n}_{aldehyde,p})} \text{ (Equation 5)}$$

Where $\dot{n}_{r,p}$ and $\dot{n}_{r,f}$ are the molar flowrates of the reactant in the product stream and feed, $\dot{n}_{aldehyde,p}$ is the molar flowrates of the aldehyde in the product stream, and $\dot{n}_{i,p}$ is the molar flowrate of species *i* in the product stream.

Another way to decrease condensation reactions is to decrease the reactant partial pressure. Since condensation reactions are typically second order with respect to the reactant and dehydration reactions are typically first order with respect to the reactant, decreasing the reactant partial pressure will increase the 1-octene selectivity. To test this hypothesis, the 1-octanol partial pressure was decreased from 7.2 psi to 3.8 psi with the resulting conversion and selectivities shown in Table 2 with and without co-feeding of H_2. At this lower partial pressure, the conversion decreased from 17% to 10% while the 1-octene selectivity increased from 38% to 56%. This would bring the normalized 1-octene selectivity to 60%, similar to the 64% for the 7.2 psi partial pressure with H_2 co-feed. At this lower partial pressure, co-feeding of H_2 decreased the 1-octene selectivity. Since the biologically derived C_8-C_{14} alcohols are 5.5 g/L (approximately 0.73 wt%) in the tridecane solvent, the alcohol partial pressures are below 0.03 psi significantly lower than 3.8 psi where the H_2 co-fed was found to be ineffective. The apparent reaction rates to 1-octene over 15%Cs/SiO_2 were 101-163 μmol/s/g_{cat} for the experiments over 50% 1-octene selectivity. These were in line with reported ethanol dehydration rates to ethylene of 220 μmol/s/g_{cat} over γ-Al_2O_3 at 215ºC in DeWilde et al. and higher than reported 2-propanol dehydration rates to propylene of 2-7 μmol/s/g_{cat} over carbon based acid catalysts at 225ºC in Bedia et al.[52, 53] Conversely, over a La-Modified HZSM-5 catalyst, Ouyang et al. reported rates >1500 μmol/s/g_{cat} for ethanol dehydration to ethylene, over an order of magnitude higher than Cs/SiO_2 but these catalysts were demonstrated with ethylene and propylene, both of which do not undergo olefin isomerization.[21] The 15%Cs/SiO_2 catalyst was selected for further investigation with the higher alcohols in simulated and biologically derived feeds due to its higher selectivity to 1-octene and lower selectivity to condensation products (8-pentadecanone and octyl octanoate).

Table 2. 1-octanol conversion and product selectivity over base dehydration catalysts with and without H_2 cofeed. Typical reaction conditions: 0.02 mL/min 1-octanol (3.8 or 7.2 psi partial pressure), 350ºC reactor temperature, 0-50 mL/min He purge gas flowrate, 0-50 mL/min H2 co-feed flowrate, 1 g catalyst, and 65 psia backpressure.

	Feed Conditions			**Conversion**	**Selectivity**						**Liquid Product**	
Catalyst	He Partial Pressure (psia)	H_2 Partial Pressure (psia)	1-octanol Partial pressure (psia)	1-octanol	1-octene	octanal	8-penta-decanone	octyl octanoate	Total known products	Normalized 1-octene[e]	Mass Balance	Carbon Balance
Blank[a]	57.5	0	7.2	0.7%[b]	7%	80%	6%	7%	100%	35%	100%	100%
15%Cs/SiO_2	57.5	0	7.2	17%	38%	4%	0%	0%	41%	40%	96%	90%
15%Cs/SiO_2	46.0	11.5	7.2	15%	51%	20%	0%	0%	74%[c]	64%	97%	96%
CeO_2	57.5	0	7.2	18%	4%	2%	17%	16%	39%	4%	100%	89%
CeO_2	46.0	11.5	7.2	18%	4%	14%	25%	44%	88%[d]	5%	96%	98%
Yb_2O_3	57.5	0	7.2	11%	3%	0%	0%	2%	5%	3%	99%	89%
Yb_2O_3	46.0	11.5	7.2	10%	2%	24%	0%	9%	36%	3%	99%	94%
15%Cs/SiO_2	60.9	0	3.8	10%	56%	6%	0%	0%	62%	60%	95%	96%
15%Cs/SiO_2	48.7	12.2	3.8	9%	53%	13%	0%	0%	65%	61%	96%	97%
15%Cs/SiO_2	36.5	24.4	3.8	10%	49%	7%	0%	0%	56%	53%	96%	96%
15%Cs/SiO_2	0	60.9	3.8	11%	42%	14%	0%	0%	57%	49%	94%	95%

a. No catalyst present and reactor tube was filled with quartz chips to reduce void space in reactor
b. Conversion was determined by products formation
c. includes 2% selectivity to trans-2-octene, 1% to cis-2-octene, and 1% to octane
d. includes 1% selectivity to octane
e. Assuming 1-octanol/octanal are in equilibrium over the catalyst

Dehydration of higher alcohols

The biologically produced feed contains primarily mixtures of even C_8-C_{14} primary alcohols. Higher alcohols such as 1-dodecanol and 1-tetradecanol are solid at room temperature and pose potential issues when pumping the feed, vaporizing the feed, and collecting the products. To demonstrate the feasibility of our system with higher chain length alcohols, the dehydration of mixed alcohols, including 4 wt% 1-octanol, 38 wt% 1-decanol, and 8 wt% 1-tetradecanol with the balance being undecane, was studied as shown in Figure 3. This ratio corresponds to the ratios produced biologically in Mehrer et al while for simplicity purposes, the 1-dodecanol was substituted with additional 1-decanol. To ensure the feed was liquid at room and condenser temperatures, an inert solvent, undecane (50 wt%) was used.[18] An alkane solvent was used for extraction of the alcohols from the fermentation broth as described in the Alcohol Production Culture subsection of the Experimental section. The preheating zone temperature was increased to 300ºC from 200ºC to ensure vaporization of all the alcohols prior to the catalyst bed while the condenser temperature was raised to 6ºC from 0ºC to help prevent solid formation during collection. A He purge gas flowrate was adjusted to 25 mL/min to maintain a total alcohol partial pressure of 3 psi to be consistent with the conditions found from the 1-octanol studies.

The experimental results are displayed in Figure 3 highlighting the alcohol conversions, 1-alkene selectivity, and aldehyde selectivity. The conversions increased from 9.1% with the neat 1-octanol feed to 11.4%, 23.7%, and 38.6% for 1-octanol, 1-decanol, and 1-tetradecanol respectively. This suggests that the higher alcohols have higher rates of dehydration. Additionally, the selectivity to 1-alkenes increased from 56.4% with neat 1-octanol to 83.4, 77.4, and 99.3% selectivity respectively to 1-octene, 1-decene, and 1-tetradecene. It is unknown what specifically increased the 1-alkene selectivity, it is possible that higher alcohols have a lower propensity to form side products while the 1-octanol was at a low enough partial pressure to minimize side products. There was no detectable octanal, while the 1-decanal selectivity was 6.3% and the 1-tetradecanal selectivity was 2.1%. The normalized 1-alkene selectivity is 83.4%, 82.7%, and 101.4% for 1-octanol, 1-decanol and 1-tetradecanol respectively.

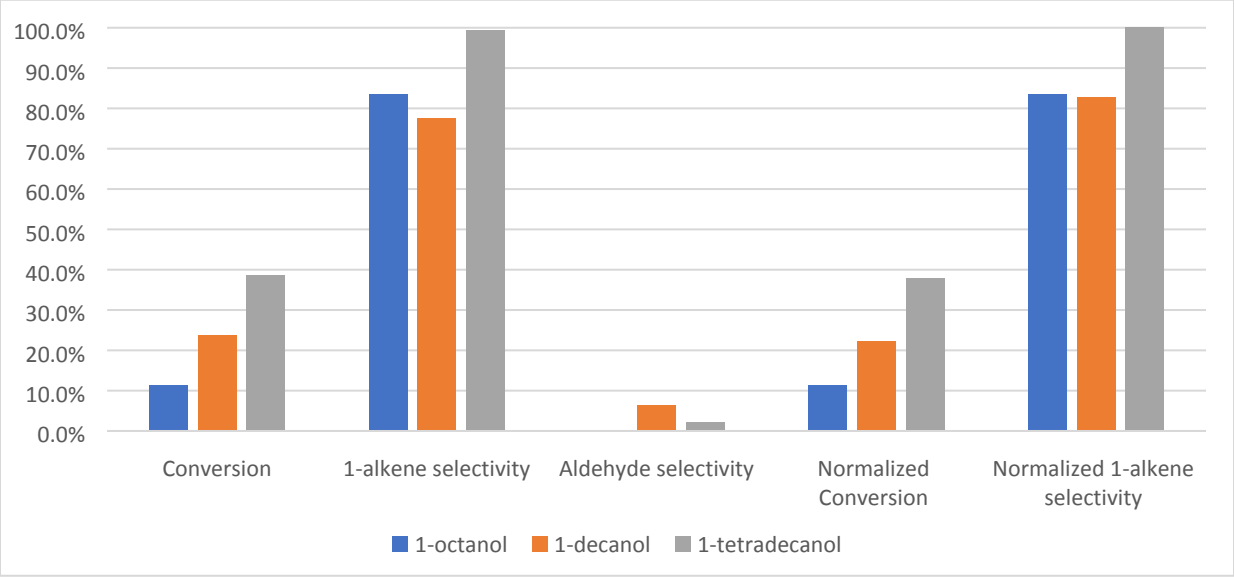

Figure 3. Conversion, product selectivity, normalized conversion, and normalized 1-alkene selectivity of mixed alcohol feed containing 4% (0.29 psia) 1-octanol, 38% (2.72 psia) 1-decanol, 8% (0.57 psia) 1-tetradecanol, and 50% (3.58 psia) undecane by weight. Normalized conversion and normalized 1-alkene

selectivity assume the aldehydes are in equilibrium with the alcohols over the catalyst. Reaction conditions: 0.02 mL/min feed flowrate, 350ºC reactor temperature, 25 mL/min He purge gas flowrate, 1 g 15%Cs/SiO_2 catalyst, and 65 psia backpressure.

Additionally, the even carbon C_8-C_{12} 1-alkanols were tested separately for dehydration over the 15%Cs/SiO2 catalyst as shown in Table 3. The 1-alkanols were dissolved to 50 wt% in tridecane for the experiments since 1-dodecanol is a solid at room temperature. 1-octanol had a 11% conversion and 46% selectivity to 1-octene. 1-decanol and 1-dodecanol showed increased LAO selectivity at 54% and 65% at conversions of 18% and 12% respectively. 1-dodecanol had to be further diluted in tridecane due to pumping issues from the higher viscosity. Similarly, 1-tetradecanol was having viscosity issues and was not tested at these higher concentrations.

Table 3: Comparison of 1-alkanol dehydration over 15%Cs/SiO_2. Reaction conditions: 0.02 mL/min feed (50% 1-alkanol, 50% tridecane by mass), 350ºC reactor temperature, 25 mL/min He purge gas flowrate, 1 g catalyst, and 65 psia backpressure.

	Feed Conditions			**Conversion**	**Selectivity**		**Liquid Product**	
Feedstock	He partial pressure (psi)	1-alkanol partial pressure (psi)	Tridecane partial pressure (psi)	1-alkanol	1-alkene selectivity	Aldehyde selectivity	Mass Balance	Carbon Balance
1-octanol	59.0	3.51	2.48	11	46	7	96.4%	96.4%
1-decanol	61.0	2.16	1.84	18	54	4	98.4%	98.4%
1-dodecanol	59.1	0.29	5.61	12	65	20	99%	99%

Dehydration of the simulated feed and biologically derived feed

A feed which better simulated the alcohols concentrations of the biologically derived feed was tested to get a baseline for how it would work with the biologically derived feed. The simulated feed was composed of 0.38 g/L 1-octanol, 1.40 g/L 1-decanol, 1.42 g/L 1-dodecanol, and 1.04 g/L 1-tetradecanol in a tridecane as displayed in Table 4. The simulated feed was modelled after the products in Mehrer et al. although dodecane was substituted for tridecane as to reduce overlap with 1-dodecanol dehydration products.[18] Compared to the mixed alcohol feed, the simulated feed has lower alcohol concentrations and the catalyst mass was adjusted to 50 mg from 1 g to compensate. The simulated feed had conversion and 1-alkene selectivity as displayed in Figure 4(a) and Figure S1(a). Samples were not collected between 10-22 h timepoints. The overnight time points were collected to measure the catalysts stability. The conversions decreased from 51%, 69%, 77%, and 91% at 3 h to 32%, 49%, 61%, and 77% at 30 h for 1-octanol, 1-decanol, 1-dodecanol, and 1-tetradecanol respectively, showing a steady deactivation rate during the reaction. 1-alkene selectivity increased from 78%, 82%, 84%, and 82% to nearly 100% for each respectively. The conversion of the alcohol increases with carbon length despite the 1-decanol and 1-dodecanol being the most abundant alcohols. No aldehyde products were detected likely due to the lower feed concentrations.

Table 4. Alcohol concentrations in Simulated Feed and Biologically Derived Feed

Compound	Simulated Feed[a]		Biologically Derived Feed	
	Concentration (g/L)	Molarity ($*10^{-3}$mol/L)	Concentration (g/L)	Molarity ($*10^{-3}$mol/L)
1-octanol	0.38	2.95	0.57	4.36
1-decanol	1.40	8.83	1.74	11.00
1-dodecanol	1.42	7.64	2.02	10.90
1-tetradecanol	1.04	4.73	1.18	5.35

a. Concentrations modelled after Mehrer et al.[18]

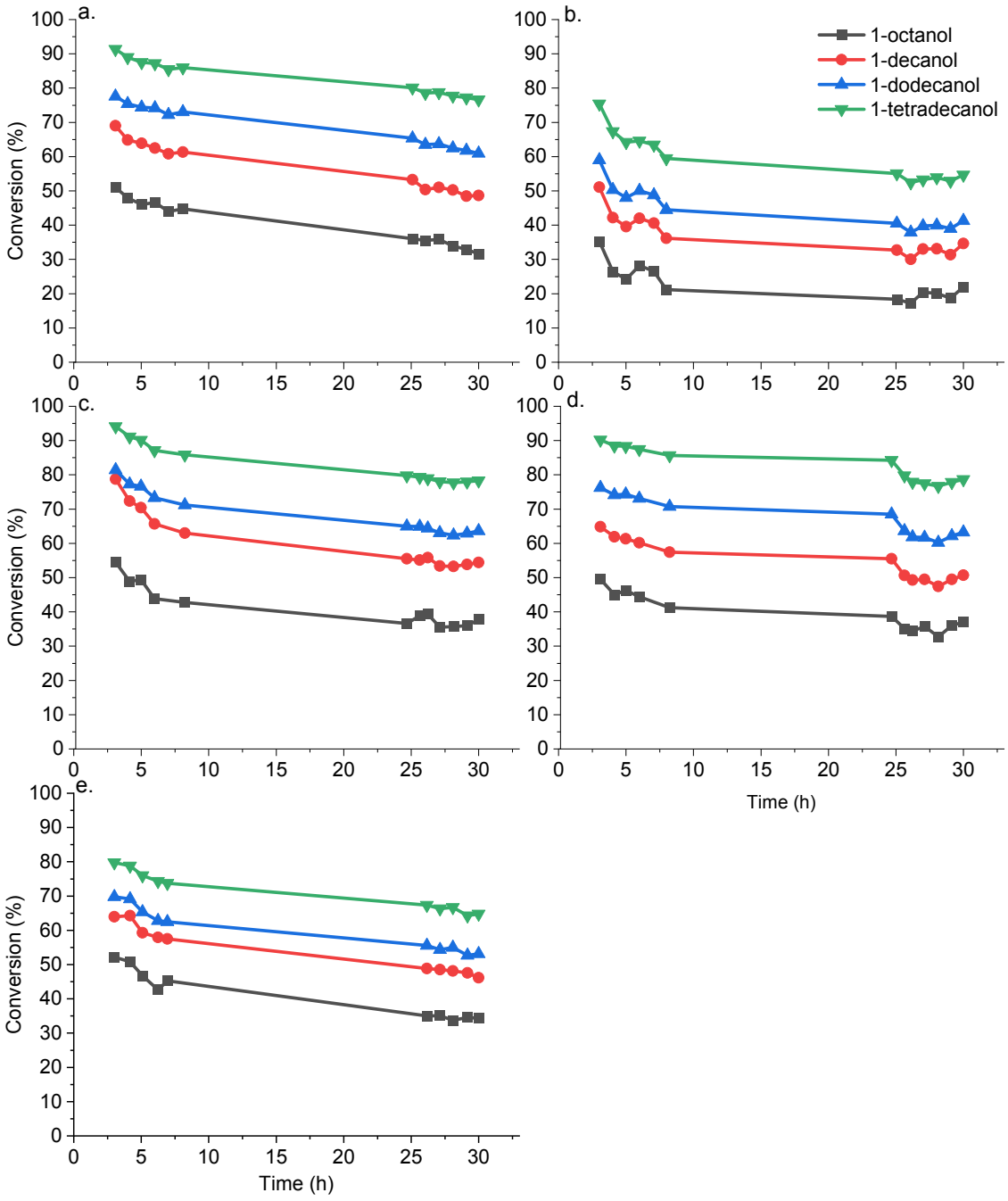

Figure 4. Conversion of a. simulated primary alcohol feed, b. biologically derived alcohol feed, c. simulated primary alcohol feed doped with C_8 and C_{10} acetate impurities, d. simulated primary alcohol feed doped with extracted LB broth components, and e. simulated primary alcohol feed doped with fatty acids. Reaction conditions: 0.02 mL/min feed flowrate, 350ºC reactor temperature, 50 mL/min He purge gas flowrate, 50 mg 15%Cs/SiO_2 catalyst, and 65 psia backpressure.

Following the experiments with the simulated feed, experiments with the biologically derived feed were performed and displayed in Figure 4(b) and Figure S1(b). The biologically derived feed displayed deactivation of the catalyst with a downward trend in the conversion decreasing from 35-75% at the 3 h to 22-55% at the 30 h for the four alcohols, showing the catalyst has a lower initial activity but similar deactivation of sites. With the decrease in conversion, selectivity to alpha olefins fluctuated between 60 and 100% during the 30 h. This deactivation was attributed to impurities in the biologically derived feed and upon inspection, several types of compounds were identified as potential culprits. The deactivation was hypothesized to be caused by one or more of the following impurities in the biologically derived feed, i) acetic acid esters, ii) fatty acids, or iii) growth media components. Acetic acid esters were discovered in the biologically derived feed with GC-MS and were detected at 0.11 g/L with GC-FID. Intermediate fatty acyl species and lipids were quantified via FAME analysis using previously described methods with only the tridecane feed.[54] The concentration and was found to be at least 0.18 g/L of mixed lipid and fatty acid species (Figure S2). The growth media components have not been directly identified in the biologically derived feed but it is possible that mineral or other compounds are present in small quantities. The acids and esters can be particularly troublesome since they could directly react with the catalytic base sites, blocking them and preventing further facilitation of the dehydration reactions.

To investigate which impurities in the biologically derived feed causes the deactivation of catalyst, several reactions were conducted with simulated feed doped with impurities. With the GC-MS analysis, acetic acid esters in the biologically derived feed were confirmed to be 0.07 g/L of decyl acetate and 0.04 g/L of lauryl acetate. Thus, 0.07 g/L of decyl acetate and 0.04 g/L of lauryl acetate were added into the simulated feed. The results for the simulated feed doped with acetic acid esters are shown in Figure 4(c) and Figure S1(c). It shows the deactivation of catalyst with the decreasing conversion from 54-94% at 3 h down to 38-78% at 30 h for the alcohols, which is similar with the deactivation of catalyst in the simulated feed (51-91% at 3 h and 32-77% at 30 h). This indicates that acetic acid esters do not contribute to the deactivation of catalyst with the biologically derived feed.

Next, the growth media components in the biologically derived feed were tested for contributions to deactivation. Lysogeny broth, which is a nutritionally rich medium for the growth of *E. coli*, supplemented with 1% glucose and appropriate antibiotics was added mixed with tridecane for 24 hours in a baffled flask in a rotary shaker at 250 RPM and 30ºC to encourage mixing. After 24 hours, the aqueous phase was removed, and the organic phase was taken with the four alcohols added. An experiment with the resulting feed was conducted and compared to the simulated feed. The 30-hour reaction results are presented in Figure 4(d) and Figure S1(d). It displays the deactivation of catalyst from 50-90% of conversion at 3 h down to 37-79% of conversion at 30 h for the all alcohols, which has the similar trend with that in the simulated feed (51-91% at 3 h and 32-77% at 30 h). This result implies that the growth media components also do not cause the deactivation of catalyst. To quantify possible β-oxidation intermediate fatty acyl-CoAs or lipid components, we applied FAME analysis to the biologically derived feed (Figure 13).

To simulate the effect of these species we doped a simulated feed with 0.05 g/L of hexadecanoic acid and 0.01 g/L of octanoic acid for a 30-hour reaction, as presented in Figure 3(e) and Figure S1(e). For the C8 and C10 alcohols, the conversion with the simulated feed doped with fatty acids exhibits similar values with the ones with the simulated feed. However, for the C_{12} and C_{14} alcohols, the initial conversion with the simulated feed doped with fatty acids decreased around

10%, indicating that the catalyst has lower initial activity due the addition of fatty acids. Similar to the real feed, the catalyst exhibits deactivation similar to the simulated feed during the course of the reaction. Additionally, the selectivity to LAOs for the four alcohols in the simulated feed doped with fatty acids all decrease (10 – 15%) after the 30-hour reaction, which results in the lower yields. We can conclude that the fatty acids in the biologically derived feed poison the active sites on the catalysts, causing the catalysts initial lower catalytic activity. However, comparing the extent of degradation between the simulated feed doped with fatty acids and the real feed, it shows that the catalysts initial activity is even further depress with the real feed. This suggests that there might be other substances in the real feed, which are not detectable by GC-MS, poisoning the active sites on the catalysts.

Regeneration of the catalysts was investigated with the simulated feed. First, the fresh catalyst was run for 30 h. After the reaction, the spent catalyst was calcined under the flow of 100 mL/min air with a 1ºC/min ramp to 450ºC and a 240 min hold followed by cooling to room temperature. Afterwards, another 30-hour experiment with the simulated feed was conducted out with the results shown in Figure 5. For the fresh catalyst, the conversions for four alcohols are initially 47-89% and decrease to 33-78% after 30-hour reaction. After regeneration, the conversions nearly reach their initial conversion at 49-90% and decrease to 37-77% after the 30 h experiment, indicating that the poisoned catalysts can most be regenerated through calcination of the catalyst. Additionally, the selectivities of the fresh and regenerated catalysts exhibit similar trends. These results suggest that the main form of deactivation of the catalysts can be attributed to the coke formation which is removed through calcination.

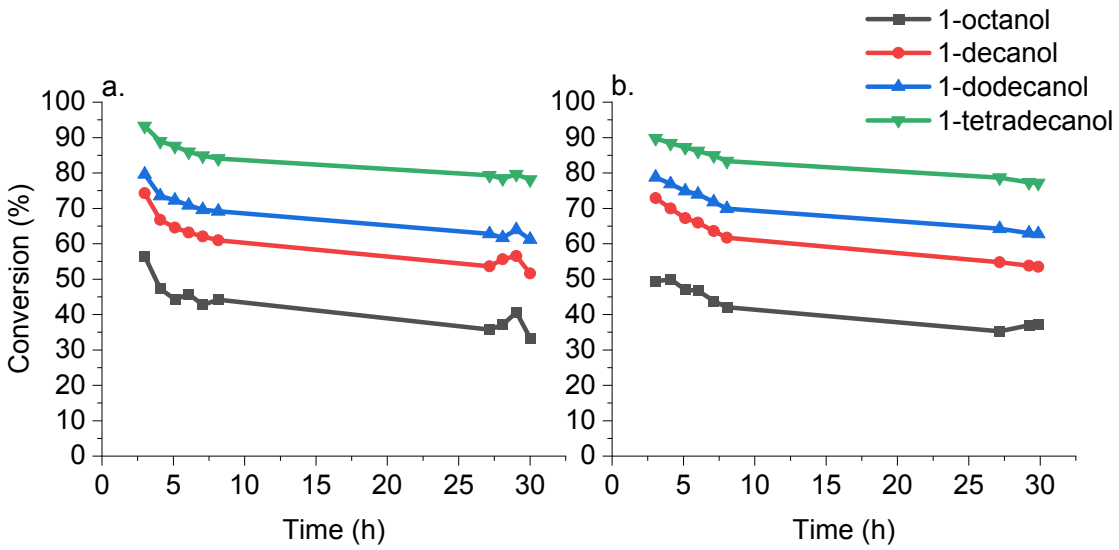

Figure 5. Conversion of simulated primary alcohol feed with a. fresh catalyst and b. regenerated catalyst. Reaction conditions: 0.02 mL/min feed flowrate, 350ºC reactor temperature, 50 mL/min He purge gas flowrate, 50 mg 15%Cs/SiO2 catalyst, and 65 psia backpressure.

Catalyst Characterization

CO_2 temperature programmed desorption (CO_2 TPD), NH_3 temperature programmed desorption (NH_3 TPD), Scanning transmission electron microscopy (STEM), and X-ray Photoelectron Spectroscopy (XPS) were utilized to characterize the catalyst. The CO_2 TPD is shown in Figure 6(a: 15%Cs/SiO_2, and b: Ce_2O_3 and YbO_2) and highlights the base sites of the

catalysts. The 15%Cs/SiO_2 catalyst has 32.3 µmol base sites/g cat, of those 31.9 µmol base sites/g cat are weak base sites primarily in a peak around 125ºC. Additionally, there was 0.4 µmol base sites/g cat of strong base sites, distributed throughout the 200-700ºC range. This agrees with Brentzel et al. in that the base sites are primarily weak but they found only 7.4 µmol base sites/g cat signifying that our catalyst had a higher dispersion of the Cs.[33] The 15%Cs/SiO_2 catalyst observed some changes in the base sites after reaction. The spent 15%Cs/SiO_2 catalyst had 30.9 µmol base sites/g cat with 26.0 µmol base sites/g cat of weak base sites in a peak around 125ºC and 4.9 µmol base sites/g cat of strong base sites in a peak around 475ºC. The minimal change in the total number of base sites of the 15%Cs/SiO_2 alludes that the deactivation during reaction is not from poisoning of the catalyst. The change base sites from weak to strong could be the more likely culprit in catalyst deactivation. The CeO_2 catalyst had two distinct peaks at 127ºC and 614ºC with a stretch of base sites between them. The 127ºC accounted for 148.4 µmol base sites/g cat and the 614ºC accounted for 70.6 µmol base sites/g cat with 46.8 µmol base sites/g cat in the stretch between them. The Yb_2O_3 had no distinct peaks with CO_2 desorbing fairly consistently from 40 to 700ºC with a total of 6.0 µmol base sites/g cat, almost two orders of magnitude lower than CeO_2. Aldol condensation has been reported to be catalyzed over weak, medium, and strong base sites while selective primary alcohol dehydration has been noted to be favored over weak base sites.[33, 55-57] Strong base sites have been shown to selectively catalyze secondary alcohol dehydrations to primary alcohols.[58] NH_3 TPD was also carried out on the catalysts to investigate the acid sites. The pure SiO_2 support was found to have around 20 µmol acid sites/g cat while the 15% Cs/SiO_2 was found to have no acid sites. This indicated that the Cs is at least partially depositing on the SiO_2 acid sites neutralizing or blocking the sites. This is beneficial for alcohol dehydration since acid sites are not desired for selective alcohol dehydration. Although acid sites also facilitate the desired dehydration reactions, they cause a scrambling of the double bond location through isomerization reactions. Both CeO_2 and Yb_2O_3 were not found to have any acid sites which is verified through the reaction products for all catalysts since no isomerization of 1-octene was present.

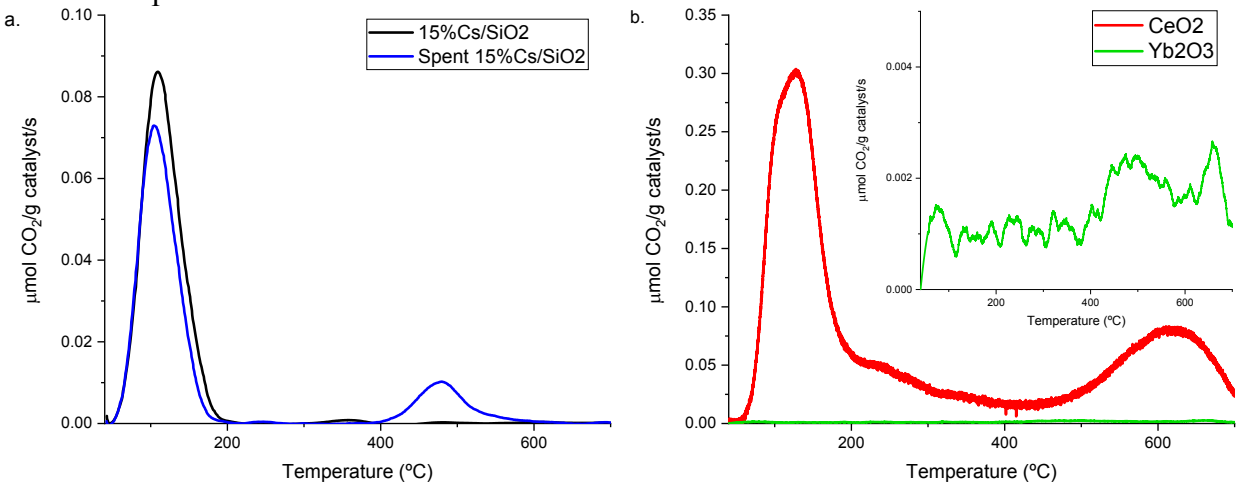

Figure 6. CO_2 TPD of a. fresh and spent 15% Cs/SiO_2 and b. CeO_2 and Yb_2O_3 catalysts for highlighting base site quantity and strength.

STEM was used to image the 15%Cs/SiO_2 catalyst. An example of one of the STEM images of the 15%Cs/SiO_2 catalyst is shown in Figure 7(a) where the smaller Cs particles are dispersed on the SiO_2 surface. The Cs particles are fairly small with an average particle diameter

of 2.31± 0.76 nm (st. dev) as shown in a particle size distributions in Figure 7(b). This is in contrary to STEM imaging in Brentzel et al. which showed Cs particles ranging from 10 nm to 85 nm. The difference in particle sizes is in agreement with the base site differences, both point to the Cs being better dispersed on our catalyst.[33] This may be due to a difference in the catalyst synthesis where during incipient wetness impregnation of CsAc on SiO_2, Brentzel et al. dried the catalyst for 2 h at room temperature prior to calcination where we dried at 110ºC for overnight (approximately 16 h) prior to calcination.[33] After the reaction, STEM of the spent catalyst does not have any apparent Cs particles on the SiO_2 support as shown in Figure 8. This indicates that the Cs is further re-dispersed during the reaction and could be the reason why a stronger basic site is observed in Figure 6.

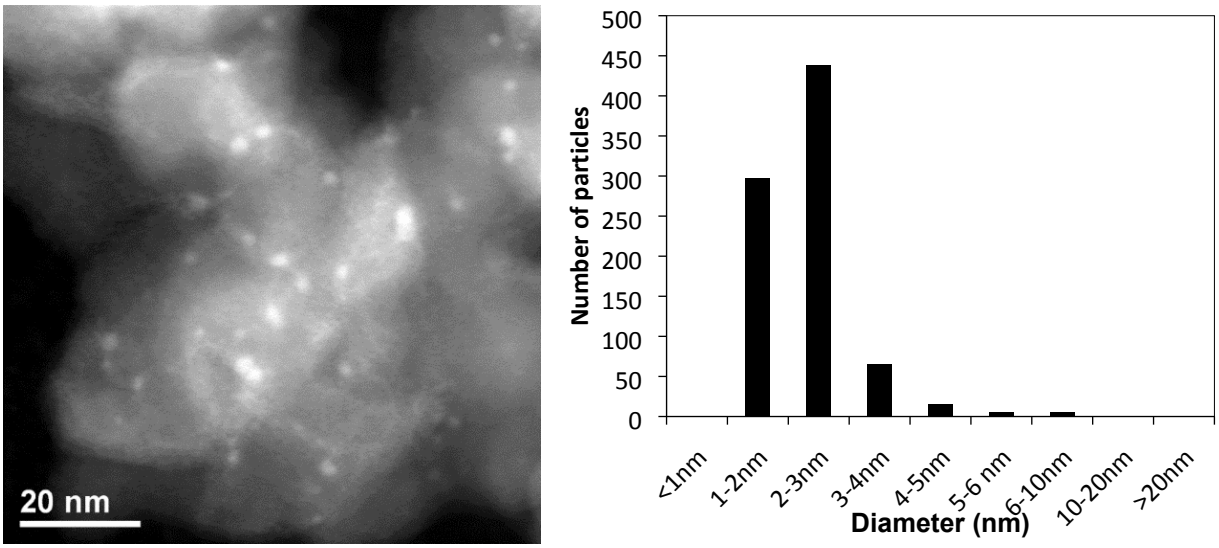

Figure 7. a. STEM image of 15% Cs/SiO_2 catalyst showing the particle size and dispersion of the Cs on the SiO_2 support. b. Particle size distribution of 15%Cs/SiO2 from STEM images. $D_{average}$ = 2.31± 0.76 nm (st. dev), 828 Cs particles analyzed.

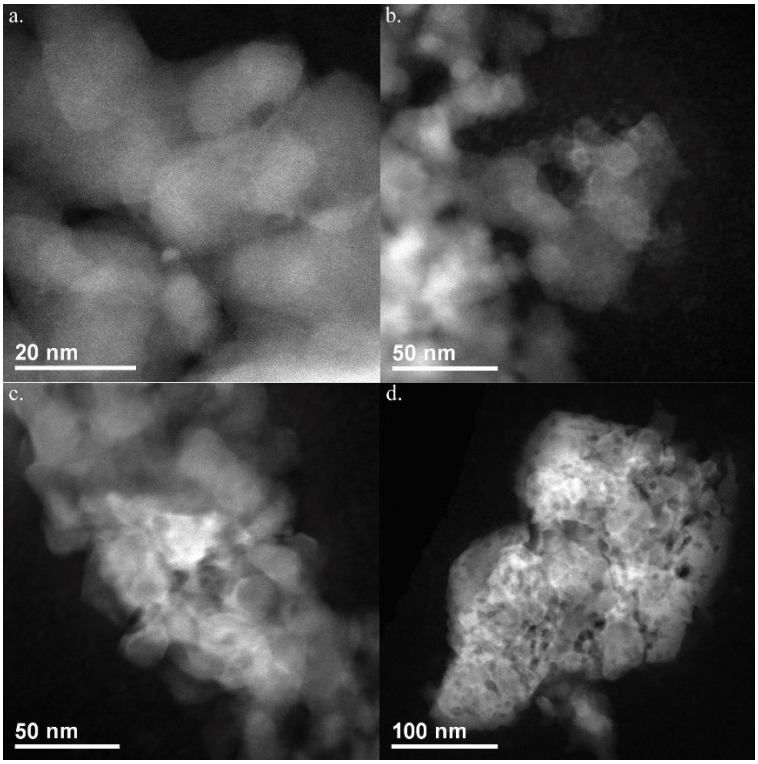

Figure 8. Four STEM images of spent 15% Cs/SiO_2 catalyst showing absence of defined Cs_2O particles on the SiO_2 support.

XPS was also conducted on the fresh and spent 15%Cs/SiO_2 catalysts as shown in Figure 9. The fresh catalysts was pretreated in He similar to the reaction pretreatment while the spent catalysts were analyzed after drying with He. XPS was conducted on four catalyst samples, fresh catalyst without air exposure, fresh catalyst with air exposure, spent catalyst from a simulated feed experiment, and spent catalyst from a biological feed experiment. Air exposure does not appear to affect the results indicating the Cs was not in the carbonate form, which could happen spontaneously in air through picking up CO_2. Cs species were suggested to be at Cs(I) state.[59] After the calcination during the Cs/SiO_2 synthesis, the Cs should be in the form of Cs_2O though it is known to pick up H_2O forming CsOH. Since Cs_2O has been noted in literature to be the base site, facilitating dehydration and dehydrogenation reactions, it is likely the Cs is predominately Cs_2O.[33, 60] Both the spent catalysts appeared similar without any major difference from the fresh catalysts, where Cs(I) is the major species over the surface and no carbonates are present. The different shape between biological feed and simulated feed is probably due to a surface charge accumulation over the non-conducting surface during data-acquisitions.

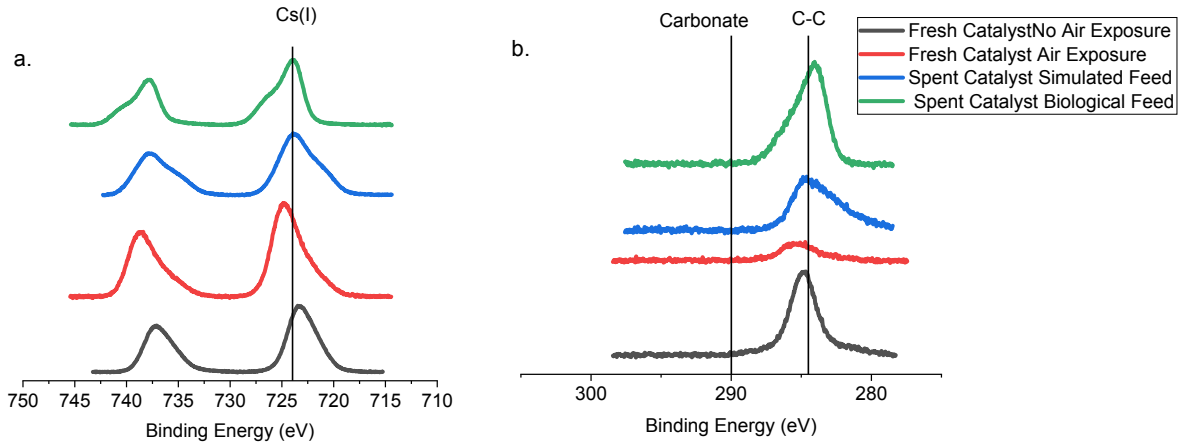

Figure 9. XPS of 15%Cs/SiO2 catalyst highlights the absence of carbonate of the fresh catalyst with and without air exposure after pretreatment as well as spent catalysts in a. Cs region, b. C region

Technoeconomic Analysis

In the baseline scenario – which represents modest improvements over laboratory-scale results but generally conservative assumptions for full-scale fermentation performance (3.5 $g \cdot L^{-1}$ titer, 50% theoretical yield, 0.1 $g \cdot L^{-1}hr^{-1}$ productivity) – the MPSP of LAOs was 3350±275 (average ± standard deviation) $USD \cdot ton^{-1}$. Given that market prices for LAOs (averaged across C_6, C_8, and C_{10}) ranged from 1080 to 1533 $USD \cdot ton^{-1}$ from 2007-2019, this baseline scenario is not financially viable. However, with fermentation improvements, financially viable LAO production could be achieved. For instance, the target scenario (40 $g \cdot L^{-1}$ titer, 80% theoretical yield, 0.5 $g \cdot L^{-1}hr^{-1}$ productivity) achieved an MPSP of 1390±172 $USD \cdot ton^{-1}$. The uncertainty of MPSP in these reported results is solely a product of the uncertainty in the cost of glucose, reinforcing the importance of glucose pricing and the potential for economically competitive, biologically derived LAOs with additional technological developments and efficient supply chains.

For the baseline fermentation performance scenario, the total capital investment is 916 MM·USD and the variable and fixed operating costs are 384±39 and 17.9 $MM \cdot USD \cdot yr^{-1}$, respectively. For the target scenario, the total capital investment is 207 MM·USD and the variable and fixed operating costs are 162±25 and 6.88 $MM \cdot USD \cdot yr^{-1}$, respectively. By achieving increases in titer from 3.5 $g \cdot L^{-1}$ to 40 $g \cdot L^{-1}$, the flow of water and solvent through the system would be greatly reduced, decreasing the total capital investment and the utility requirements of downstream separations. Even at a titer of 40 $g \cdot L^{-1}$, the product flow rate is a small fraction of the tridecane solvent being recycled through the system, as depicted by the Sankey diagram (Figure 10). Despite the large solvent recycle, the economics in the target scenario are limited by the material cost of the glucose feedstock (149±25 $MM \cdot USD \cdot yr^{-1}$), which accounts for 71±12% of the MPSP. The flow rates and compositions of all streams and the process flow diagrams for each area are available in Tables S42-S51 and Figures S3-S7.

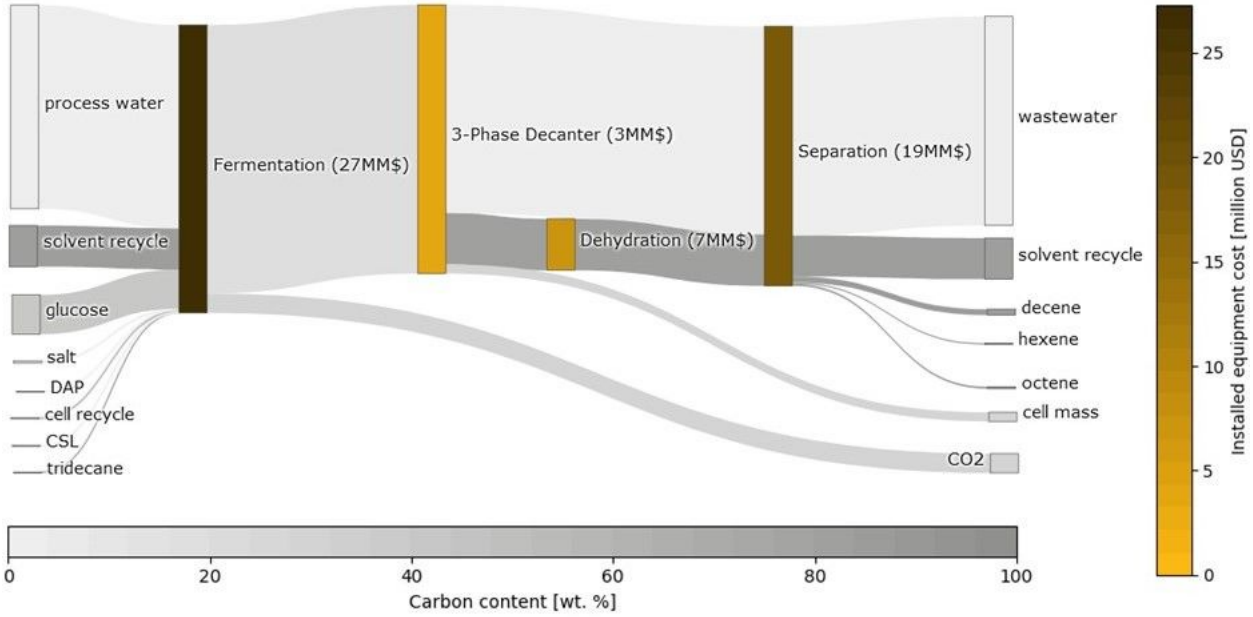

Figure 10. Sankey diagram of the material flow for production of 150,000 ton·yr^{-1} of LAOs from dehydration of glucose-derived fatty alcohols at a target fermentation performance (40 g·L^{-1} titer, 80% theoretical yield, 0.5 g·L^{-1}hr^{-1} productivity). To simplify the diagram, recycle loops are not displayed. The widths of the streams are proportional to the mass flow rate and the darkness of each stream shows carbon concentration (bottom grey scale bar). The nodes represent each area of the production process with labels and color (right orange scale bar) detailing the installed equipment costs of the units in the area.

The main sources of cost in the production process in the target scenario – including installed equipment cost, cooling duty, heating duty, and electricity consumption – are shown in Figure 11Figure 10. Because all utilities (steam, cooling water, chilled water, and electricity) are produced on-site, there is no direct utility cost associated with the production process. Instead, the cost of utility usage is reflected in the capital cost of the utility generation systems and the material cost of natural gas (Table S4 and Table S5, ESI). The cooling duty and electricity requirements from the OSBL area primarily come from the Boiler-Turbogenerator's condensing turbine and the chilled water generation system (which consume a significant fraction of the cooling water) and the cooling tower (which consumes electricity to recirculate the cooling water). The detailed design, installed equipment cost, and utility requirements for all unit operations can be found in Table S8-S41 (ESI). The separation section has the highest heating and cooling duty requirement, consistent with the need to separate and purify dilute LAO streams. The fermentation section, which consists of 13 batch reactors of 1 MGal each (Table S1, SI), has the highest capital cost contribution.

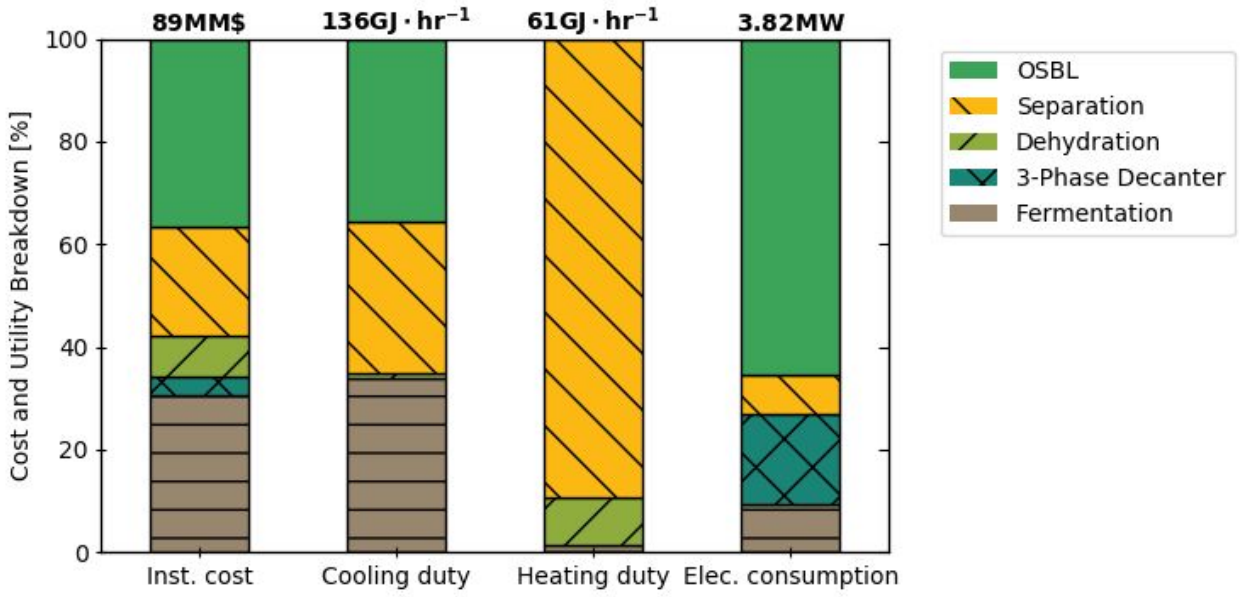

Figure 11. Contributions to installed equipment cost, cooling duty, heating duty, and electricity consumption by area for production of 150,000 ton·yr^{-1} of LAOs in the target scenario (fermentation with 40 g·L^{-1} titer, 80% theoretical yield, 0.5 g·L^{-1}hr^{-1} productivity). OSBL contributions are primarily derived from generating cooling and heating utilities. The separation section has the highest heating and cooling duty requirements. The fermentation section has the highest capital cost contribution.

The BioSTEAM software was used to evaluate the landscape of possible fermentation performance across titers, yields, and productivities to elucidate the impact of these parameters on MPSP, variable operating cost (VOC), and fixed capital investment (FCI; Figure 12). At low titers, the contour lines show that increasing titer has the largest economic benefit by significantly reducing both capital cost and operating costs. However, the marginal benefit of increasing titers above 40 $g \cdot L^{-1}$ diminishes as the cost of glucose becomes the most significant driver of MPSP. Increasing yield decreases the amount of glucose in solution required to achieve a given titer, thereby decreasing the material cost of glucose, but has no significant impact on capital cost as the molar volume of glucose in solution is negligible. Industrial fermentation processes typically operate at yields between 80-95%, thus a yield of 80% is a reasonable target for the production of fatty-alcohols. The productivity solely impacts the reactor size required to achieve a given titer and has no impact on the variable operating cost. Increasing productivity will introduce savings in capital investment, but beyond 0.5 $g \cdot L^{-1} hr^{-1}$ the savings are marginal.

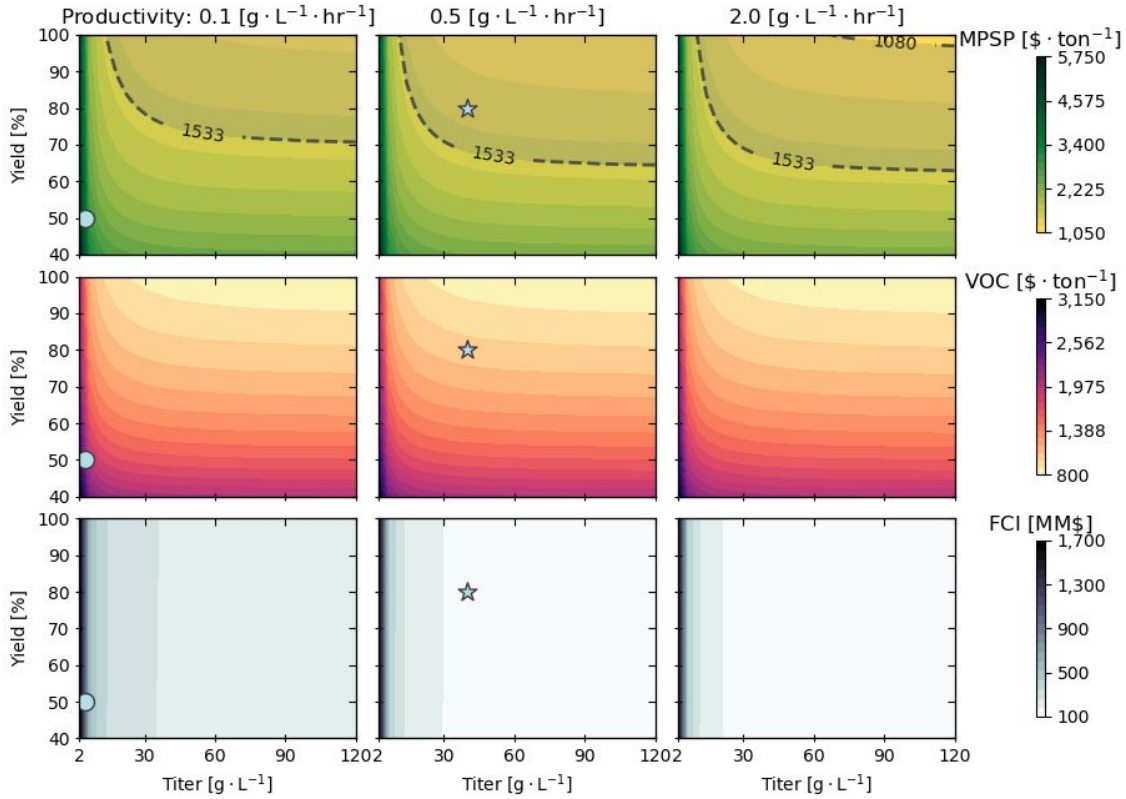

Figure 12. Contour plots of minimum product selling price (MPSP; top), variable operating cost (VOC; middle), and fixed capital investment (FCI; bottom) as a function of fermentation yield and titer across three productivities (left to right: 0.1, 0.5, and 1.0 $g \cdot L^{-1} \cdot hr^{-1}$). The circles represent the baseline scenario (conservative assumptions about fermentation performance; 3.5 $g \cdot L^{-1}$, 50% theoretical yield, 0.1 $g \cdot L^{-1} hr^{-1}$), and the stars represent a potential target scenario with industrially relevant fermentation performance (40 $g \cdot L^{-1}$, 80% theoretical yield, 0.5 $g \cdot L^{-1} hr^{-1}$).

LAO production increases in recent years have been partially supported by leveraging low-cost shale-based natural gas in the USA, the price of which will continue to influence market prices. Moving forward, the consumption of alpha-olefins is projected to continue to grow globally, with opportunities for increased production by greater than 1.6 million tons from 2019 to 2024. Ultimately, the competitiveness of biologically derived LAOs will be dependent on competing fossil-derived products, and will also require technological advancements such as those evaluated here in the target scenario.

Conclusions

LAOs can be produced by gas phase dehydration of biologically derived C_8-C_{14} 1-alkanol feed (5.5 g/L) with 60-100% LAO selectivity over a 15%Cs/SiO_2 catalyst. Feedstocks including fatty acid impurities were shown to have lower initial activity, but neither fatty acids, acetic acid esters, nor LB broth components had an impact on deactivation. The catalyst was found to be regenerable through calcination though the catalyst surface changed from 2-3 nm Cs_2O particles to what appeared to be a more dispersed Cs_2O layer on the SiO_2 surface after reaction. The dehydration conversion was demonstrated to be effective at higher concentrations with 50 wt% mixed alcohol feed and neat 1-octanol with similarly high conversions and selectivity. The main side product is the aldehyde which is in equilibrium with the alcohol, though it is undesired if it undergoes aldol condensation reactions, forming condensation products. The 15%Cs/SiO_2 catalyst was shown to primarily consist of weak base sites while a small portion stronger base sites were found on the spent catalyst. Co-feeding H_2 increased selectivity to 1-octene and octanal at higher partial pressures by inhibiting condensation products, while at lower partial pressures H_2 co-feeding decreases 1-octene selectivity.

The techno-economic analysis revealed that at the current laboratory-scale fermentation titer, the capital and operational costs would be prohibitively high due to high flows of process water and tridecane solvent throughout the system and the need to separate and purify the dilute fermentation effluent. By executing techno-economic analyses across the fermentation performance landscape, opportunities to improve the financial viability of biologically derived LAOs were characterized. At a target fermentation performance of 40 $g \cdot L^{-1}$ titer, 80% theoretical yield, and 0.5 $g \cdot L^{-1} hr^{-1}$ productivity, MPSPs in the market range could be achieved. At these improved levels of performance, glucose becomes the main driver of cost (71±12% of the MPSP at the target scenario), underscoring the need for robust supply chains to support a growing bioeconomy.

Acknowledgements

This work was funded by the DOE Center for Advanced Bioenergy and Bioproducts Innovation (U.S. Department of Energy, Office of Science, Office of Biological and Environmental Research under Award Number DE-SC0018420). Any opinions, findings, and conclusions or recommendations expressed in this publication are those of the author(s) and do not necessarily reflect the views of the U.S. Department of Energy. We would like to thank Faysal Ibrahim for his work on synthesizing catalysts as an undergraduate researcher.

References

1. S. D. Ittel, L. K. Johnson and M. Brookhart, *Chemical Reviews*, 2000, **100**, 1169-1204.
2. R. Franke, D. Selent and A. Börner, *Chemical Reviews*, 2012, **112**, 5675-5732.

3. D. Marquis, S. Sharman, R. House and W. Sweeney, *Journal of the American Oil Chemists Society*, 1966, **43**, 607-614.
4. A. Z. Elvira Greiner; Bland, E.; Kumamoto, T., *Linear Alpha-Olefins Chemical Economics Handbook.*, IHS Markit, 2020.
5. A. Al-Jarallah, J. Anabtawi, M. Siddiqui, A. Aitani and A. Al-Sa'doun, *Catalysis today*, 1992, **14**, 1-121.
6. B. L. Small and M. Brookhart, *Journal of the American Chemical Society*, 1998, **120**, 7143-7144.
7. K. Weissermel, H.-J. Arpe, C. R. Lindley and S. Hawkins, *Industrial organic chemistry*, Wiley Online Library, 1997.
8. P. Program, *Alpha Olefins(02/03-4)*, Nexant Chemical Systems, 2004.
9. S. Lee, *Encyclopedia of Chemical Processing (Online)*, CRC Press, Boca Raton, 2005.
10. Y. Liu, K. E. Kim, M. B. Herbert, A. Fedorov, R. H. Grubbs and B. M. Stoltz, *Advanced synthesis & catalysis*, 2014, **356**, 130-136.
11. F. Zamora, in *Wine chemistry and biochemistry*, Springer, 2009, pp. 3-26.
12. S. Fillet and J. L. Adrio, *World Journal of Microbiology and Biotechnology*, 2016, **32**.
13. E. R. Marella, C. Holkenbrink, V. Siewers and I. Borodina, *Current opinion in biotechnology*, 2018, **50**, 39-46.
14. J.-F. Rontani, in *Handbook of Hydrocarbon and Lipid Microbiology*, ed. K. N. Timmis, Springer Berlin Heidelberg, Berlin, Heidelberg, 2010, DOI: 10.1007/978-3-540-77587-4_34, pp. 459-470.
15. M. K. Akhtar, N. J. Turner and P. R. Jones, *Proceedings of the National Academy of Sciences*, 2013, **110**, 87-92.
16. S. Kim, J. M. Clomburg and R. Gonzalez, *J Ind Microbiol Biotechnol*, 2015, **42**, 465-475.
17. R. Liu, F. Zhu, L. Lu, A. Fu, J. Lu, Z. Deng and T. Liu, *Metab Eng*, 2014, **22**, 10-21.
18. C. R. Mehrer, M. R. Incha, M. C. Politz and B. F. Pfleger, *Metab Eng*, 2018, **48**, 63-71.
19. Y. J. Zhou, N. A. Buijs, V. Siewers and J. Nielsen, *Front Bioeng Biotechnol*, 2014, **2**, 32.
20. C. Pramod, R. Fauziah, K. Seshan and J.-P. Lange, *Catalysis science & technology*, 2018, **8**, 289-296.
21. J. Ouyang, F. Kong, G. Su, Y. Hu and Q. Song, *Catalysis letters*, 2009, **132**, 64-74.
22. R. Ermakov and V. Plakhotnik, *Petroleum Chemistry*, 2008, **48**, 1-5.
23. Y. Chen, Y. Wu, L. Tao, B. Dai, M. Yang, Z. Chen and X. Zhu, *Journal of Industrial and Engineering Chemistry*, 2010, **16**, 717-722.
24. J. W. Jun, J. Jeon, C.-U. Kim, K.-E. Jeong, S.-Y. Jeong and S. H. Jhung, *Journal of nanoscience and nanotechnology*, 2013, **13**, 2782-2788.
25. S. Sugiyama, Y. Kato, T. Wada, S. Ogawa, K. Nakagawa and K.-I. Sotowa, *Topics in Catalysis*, 2010, **53**, 550-554.
26. E. Ozdogan, T. Dogu and G. Dogu, *International Journal of Chemical Reactor Engineering*, 2007, **5**.
27. Q. Pan, A. Ramanathan, W. K. Snavely, R. V. Chaudhari and B. Subramaniam, *Topics in Catalysis*, 2014, **57**, 1407-1411.
28. Q. Pan, A. Ramanathan, W. K. Snavely, R. V. Chaudhari and B. Subramaniam, *Industrial & Engineering Chemistry Research*, 2013, **52**, 15481-15487.
29. H. Dunning, *Industrial & Engineering Chemistry*, 1953, **45**, 551-564.
30. H. Pines and J. Manassen, in *Advances in catalysis*, Elsevier, 1966, vol. 16, pp. 49-93.

31. N. Yamamoto, S. Sato, R. Takahashi and K. Inui, *Catalysis Communications*, 2005, **6**, 480-484.
32. H. Hattori, *Applied Catalysis A: General*, 2001, **222**, 247-259.
33. Z. J. Brentzel, M. R. Ball and J. A. Dumesic, *Catalysis Letters*, 2018, **148**, 3072-3081.
34. V. Solinas, E. Rombi, I. Ferino, M. G. Cutrufello, G. Colón and J. Navıo, *Journal of Molecular Catalysis A: Chemical*, 2003, **204**, 629-635.
35. P. Thomasson, O. Tyagi and H. Knözinger, *Applied Catalysis A: General*, 1999, **181**, 181-188.
36. D. Tsukamoto, S. Sakami, M. Ito, K. Yamada and T. Yonehara, *Chemistry Letters*, 2016, **45**, 831-833.
37. K. Tanabe, M. Misono, H. Hattori and Y. Ono, *New Solid Acids and Bases: Their Catalytic Properties*, Elsevier, 1989.
38. H. Chang, I. Bajaj, G. W. Huber, C. T. Maravelias and J. A. Dumesic, *Green Chemistry*, 2020, **22**, 5285-5295.
39. J. He, M. Liu, K. Huang, T. W. Walker, C. T. Maravelias, J. A. Dumesic and G. W. Huber, *Green Chemistry*, 2017, **19**, 3642-3653.
40. J. Q. Bond, A. A. Upadhye, H. Olcay, G. A. Tompsett, J. Jae, R. Xing, D. M. Alonso, D. Wang, T. Zhang, R. Kumar, A. Foster, S. M. Sen, C. T. Maravelias, R. Malina, S. R. H. Barrett, R. Lobo, C. E. Wyman, J. A. Dumesic and G. W. Huber, *Energy & Environmental Science*, 2014, **7**, 1500-1523.
41. R. Xing, A. V. Subrahmanyam, H. Olcay, W. Qi, G. P. van Walsum, H. Pendse and G. W. Huber, *Green Chemistry*, 2010, **12**, 1933-1946.
42. L. M. L. Laurens, N. Nagle, R. Davis, N. Sweeney, S. Van Wychen, A. Lowell and P. T. Pienkos, *Green Chemistry*, 2015, **17**, 1145-1158.
43. S. Sadula, N. Rodriguez Quiroz, A. Athaley, E. O. Ebikade, M. Ierapetritou, D. G. Vlachos and B. Saha, *Green Chemistry*, 2021, **23**, 1200-1211.
44. J. Byun and J. Han, *Green Chemistry*, 2017, **19**, 5214-5229.
45. J. Lee, W. Lee, K. H. Ryu, J. Park, H. Lee, J. H. Lee and K. T. Park, *Green Chemistry*, 2021, **23**, 2397-2410.
46. Y. K. Cortes-Peña, D.; Singh, V.; Guest, J. S., *ACS Sustain. Chem. Eng.*, 2020, **8**, 3302-3310.
47. D. D. Humbird, R.; Tao, L.; Kinchin, C.; Hsu, D.; Aden, A.; Schoen, P.; Lukas, J.; Olthof, B.; Worley, M.; Sexton, D.; Dudgeon, D., *Process Design and Economics for Biochemical Conversion of Lignocellulosic Biomass to Ethanol: Dilute-Acid Pretreatment and Enzymatic Hydrolysis of Corn Stover;*, DOE: NREL, 2011.
48. M. H. Cheng, H.; Dien, B. S.; Singh, V., *Biofuels Bioprod. Biorefining*, 2019, **13**, 723-739.
49. F. Baddour, K. Van Allsburg, N. Wunder, J. Yarbrough, M. Jankousky, K. Gruchalla, K. Potter, J. Schaidle, E. Tan, M. Talmadge, J. Hensley, S. Habas, L. Snowden-Swan, J. Frye, U. O. o. E. Efficiency and B. T. O. Renewable Energy, *Journal*, 2019, DOI: 10.11578/dc.20191029.1.
50. M. J. L. G. Mingting Xu, Anne-Mette Hilmen, Brandy L. Stephens, and Enrique Iglesia, *Journal of Catalysis*, 1997, **171**, 130-147.
51. S. J. M. A. Yee, and H. Idriss, *Journal of Catalysis*, 1997, **186**, 279-295.
52. J. F. DeWilde, H. Chiang, D. A. Hickman, C. R. Ho and A. Bhan, *ACS Catalysis*, 2013, **3**, 798-807.

53. J. Bedia, J. M. Rosas, J. Márquez, J. Rodríguez-Mirasol and T. Cordero, *Carbon*, 2009, **47**, 286-294.
54. N. J. Hernandez Lozada, R. Y. Lai, T. R. Simmons, K. A. Thomas, R. Chowdhury, C. D. Maranas and B. F. Pfleger, *ACS Synth Biol*, 2018, **7**, 2205-2215.
55. L. Faba, E. Díaz and S. Ordóñez, *Applied Catalysis B: Environmental*, 2012, **s 113–114**, 201–211.
56. W. Bing, L. Zheng, S. He, D. Rao, M. Xu, L. Zheng, B. Wang, Y. Wang and M. Wei, *ACS Catalysis*, 2018, **8**, 656-664.
57. Y. Zhao, M. Fan, P. Wang, C. Li, L. Wang and L. Wang, *Fuel Processing Technology*, 2020, **198**, 106250.
58. V. K. Díez, C. R. Apesteguía and J. I. Di Cosimo, *Journal of Catalysis*, 2003, **215**, 220-233.
59. J. F. Moulder, W. F. Stickle, P. E. Sobol and K. D. Bomben, *Physical Electronics*, 1995.
60. P. E. Hathaway and M. E. Davis, *Journal of Catalysis*, 1988, **116**, 263-284.